

Supporting Information  
©Wiley-VCH 2021  
69451 Weinheim, Germany

## **Eutectic Electrolyte with Unique Solvation Structure for High-Performance Zinc-Ion Batteries**

Lishan Geng,<sup>[a]</sup> Jiashen Meng,<sup>[a]</sup> Xuanpeng Wang,<sup>[b]</sup> Chunhua Han,<sup>[a]</sup> Kang Han,<sup>[a]</sup> Zhitong Xiao,<sup>[a]</sup> Meng Huang,<sup>[a]</sup> Peng Xu,<sup>[a]</sup> Lei Zhang,<sup>[b]</sup> Liang Zhou,<sup>\*[a,c]</sup> and Liqiang Mai<sup>\*[a,c]</sup>

DOI: 10.1002/anie.2021XXXXX

## Experimental Procedures

### Materials synthesis

#### Synthesis of Eutectic Electrolyte (DES)

Aniline (99 %), HCl (12 M), and ammonium persulfate (99 %) were purchased from Aladdin. 0.365 mL of aniline monomer was added into 15 mL of HCl (1.0 M) solution under stirring and cooled to 0 °C in an ice bath. After stirring for 30 mins, 5 mL of HCl (1.0 M) containing 0.228 g of ammonium persulfate was added into the above solution dropwise. The colorless solution became dark green after a few mins. When the reaction is continued for 1 h, the sample obtained were washed with deionized water and ethanol and then dried at 60 °C.<sup>[6-8]</sup>

#### Synthesis of Polyaniline (PANI) Cathode Material

Aniline (99 %), HCl (12 M), and ammonium persulfate (99 %) were purchased from Aladdin. 0.365 mL of aniline monomer was added into 15 mL of HCl (1.0 M) solution under stirring and cooled to 0 °C in an ice bath. After stirring for 30 mins, 5 mL of HCl (1.0 M) containing 0.228 g of ammonium persulfate was added into the above solution by dropwise. The colorless solution became dark green after a few mins. When the reaction is continued for 1 h, the sample obtained were washed with deionized water and ethanol and then drying at 60 °C.<sup>[6-8]</sup>

PANI based cathode was prepared by mixing PANI with acetylene black, and binder (15 mg/mL polyvinylidene fluoride/N-methyl pyrrolidone) in a mass ratio of 7:2:1. The mixture was dispersed in isopropanol to form a slurry. After stirring for 5 hours, the slurry was coated onto carbon paper and then dried at 60 °C overnight. The average loading of PANI was 1.03 mg/ cm<sup>2</sup>.

#### Electrochemical Measurements

The symmetrical Zn||Zn cells, Ti||Zn cells, and PANI||Zn ZIBs cells were assembled into CR2025-type coin cells in the Ar filled glove box using Zn foil (100 μm) as the anode and glass fiber filter (Whatman, grade GF/D) as the separator. For Ti||Zn and PANI||Zn cells, Ti foil (50 μm) and PANI based electrode were employed as the cathode, respectively. The PANI||Zn punch cells wrapped with aluminum plastic film were assembled using Zn foil (100 μm) as the anode and glass fiber filter (Whatman, grade GF/D) as the separator. Linear sweep voltammetry (LSV) were acquired using the electrochemical workstation at a scan rate of 0.1 mV s<sup>-1</sup> using three-electrode cell with platinum sheet as working electrode, graphite rod as counter electrode and a saturated calomel electrode (SCE) as reference electrode. Electrochemical impedance spectroscopy (EIS) data were acquired using the electrochemical workstation with a frequency range from 100 KHz to 0.1 Hz. The electrochemical tests were all carried out using the LAND CT2001A multichannel battery testing system. The CV profiles were tested on CHI 600e electrochemical workstation.

#### Characterizations

The ionic conductivity of DES at room temperature was tested by a DDS-307 instrument. The apparent viscosity of DES at room temperature was obtained with rotational viscosity test HAAKE MARS III (Thermofisher, USA). NMR analysis was carried out on an AVANCE III 400MHz equipment (Switzerland). Fourier transform infrared spectroscopy (FTIR) spectra were carried out using EO-SXB IR spectrometer. Raman spectra were recorded using a HORIBA HR EVO Raman system with an excitation wavelength of 633 nm. Scanning electron microscopy (SEM) images and energy dispersive spectrometer (EDS) were collected using a JEOL-7100F microscope at an acceleration voltage of 15 kV. X-ray photoelectron spectroscopy (XPS) were carried out using an ESCALAB 250Xi instrument.

#### Computational Details

Molecular dynamics simulations: Molecular dynamics (MD) simulations were carried out by LAMMPS package in order to investigate solvation structure and diffusion coefficients. The OPLS\_AA force field parameters were used to describe the interactions between EG, Zn<sup>2+</sup>, and Cl<sup>-</sup>. The velocity-verlet method was used as the integral method and the integration time step was set to 0.5 fs. The cutoff radius and the electrostatic interactions were both set to 10 Å. During MD simulation, periodic condition was used. After energy minimization of the initial structure, the system was equilibrated for 5 ns in NPT ensemble where Nose-Hoover thermostat/barostat algorithm were used to control the system temperature and pressure. The temperature and pressure were set to 298.15 K and 1 atm, respectively. After equilibrated, another 10 ns simulation was carried out in NVT ensemble to collect statistical data of the system.

Density function theory (DFT) calculation: All the structures used in density functional theory calculation were optimized by ORCA at B3LYP hybrid function with def-TZVP basis. Then a single point calculation was carried at same level. DFT-D3 method was used to describe weak interaction between molecules. The Electrostatic potential (ESP) were analyzed by Multiwfn and the ESP was drawn by VMD package.

## Results and Discussion

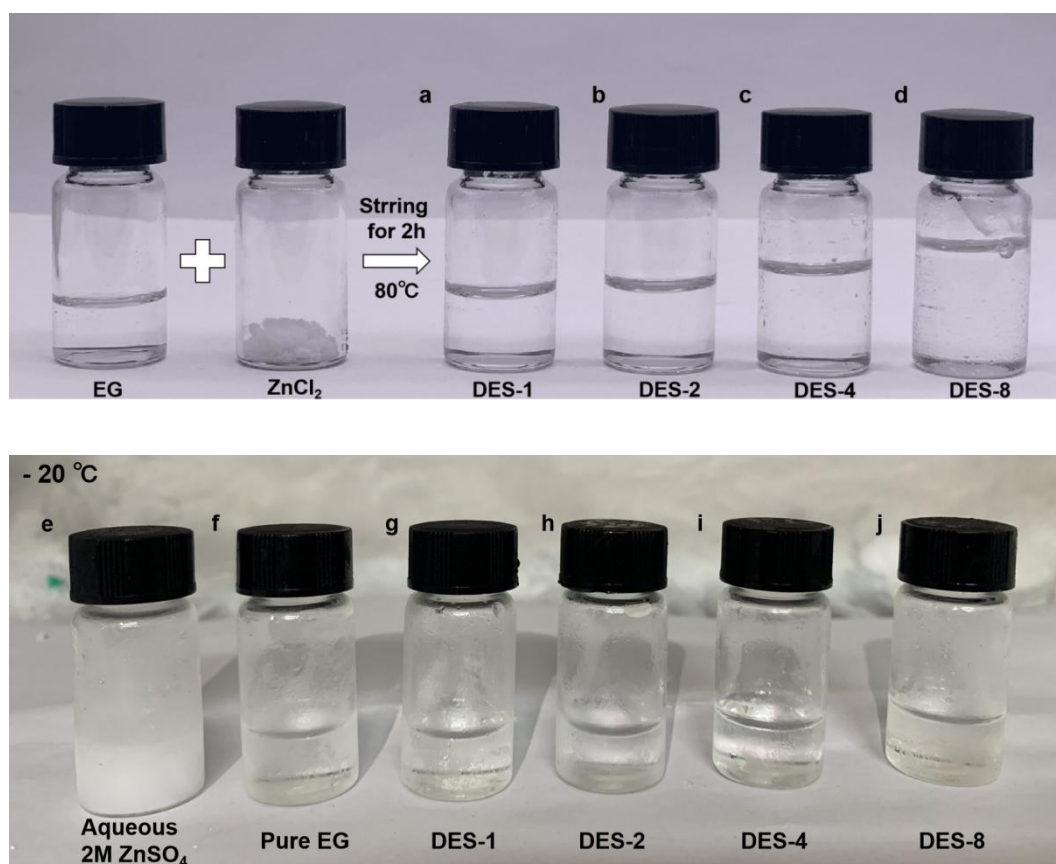


**Figure S1.** Digital photos of (a) DES-1, (b) DES-2, (c) DES-4, and (d) DES-8 at room temperature; digital photos of (e) 2.0 M ZnSO<sub>4</sub>, (f) pure EG, (g) DES-1, (h) DES-2, (i) DES-4, and (j) DES-8 at -20 °C.

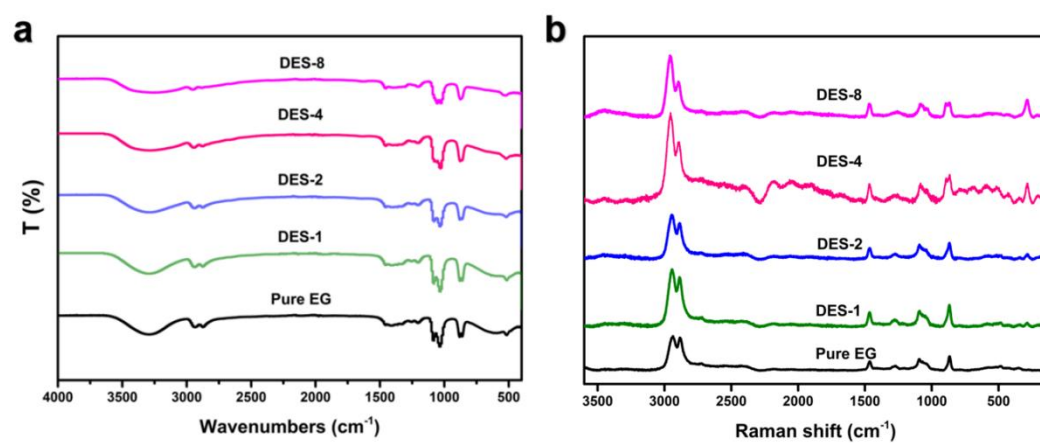


Figure S2. (a) FTIR spectra and (b) Raman spectra of DES-1, DES-2, DES-4, DES-8, and pure EG.

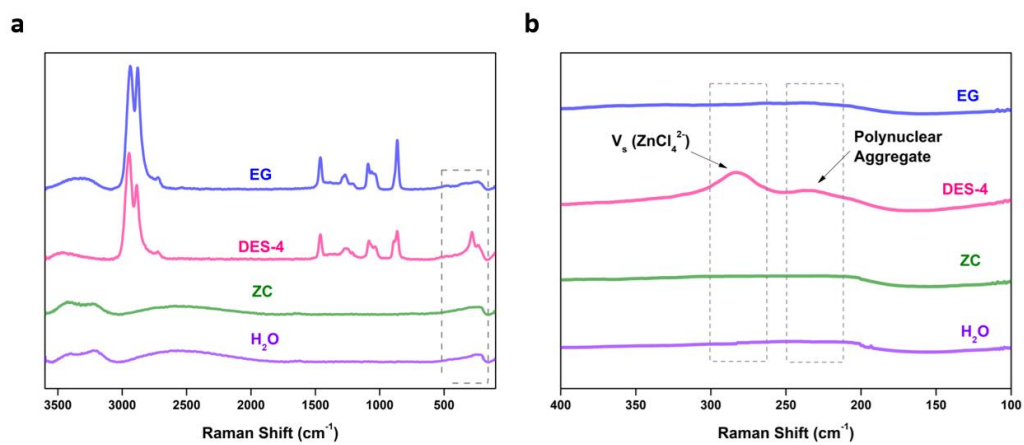


Figure S3. Raman spectra of DES-4, EG, ZC, and H<sub>2</sub>O at (a) 100-3600 cm<sup>-1</sup>, and (b) 100-400 cm<sup>-1</sup>.

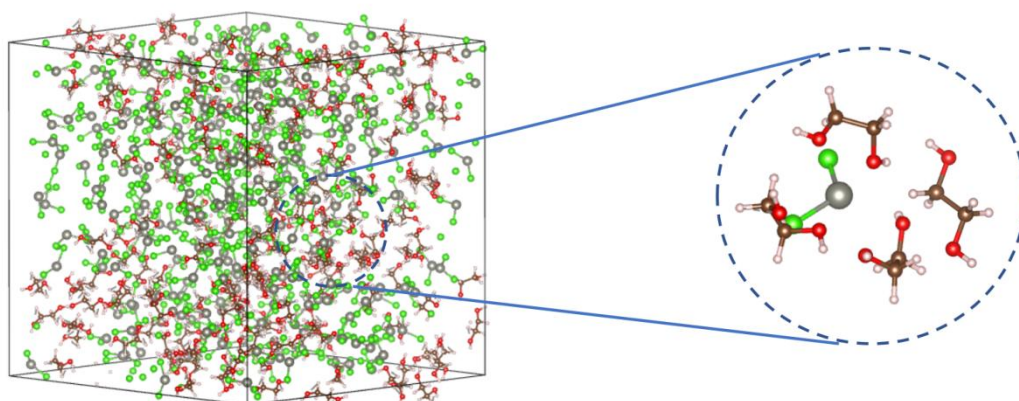


Figure S4. Snapshots of DES-1 during MD simulations.

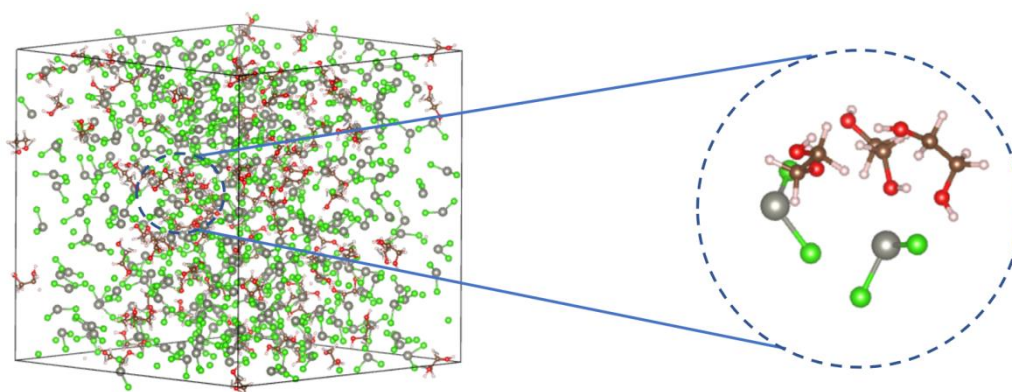


Figure S5. Snapshots of DES-2 during MD simulations.

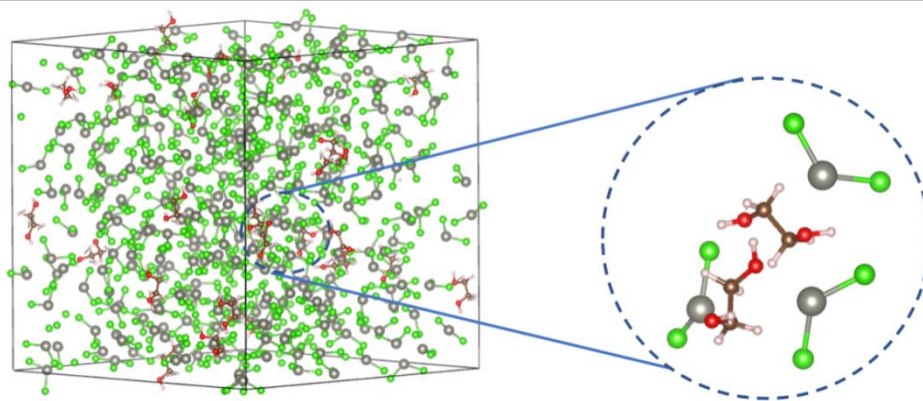


Figure S6. Snapshots of DES-8 during MD simulations.

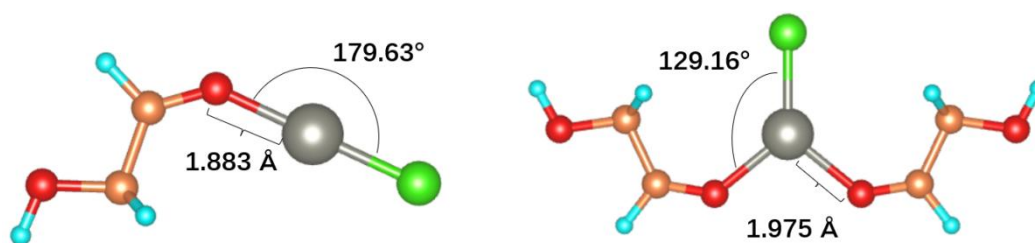


Figure S7. First coordination mode: [ZnCl(EG)]<sup>+</sup> and [ZnCl(EG)<sub>2</sub>]<sup>+</sup> cations using one -OH group of EG to coordinate with Zn<sup>2+</sup>.

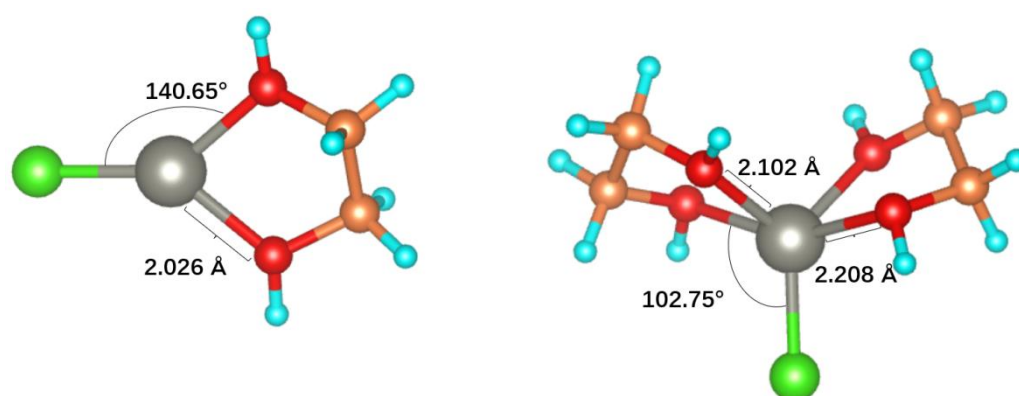
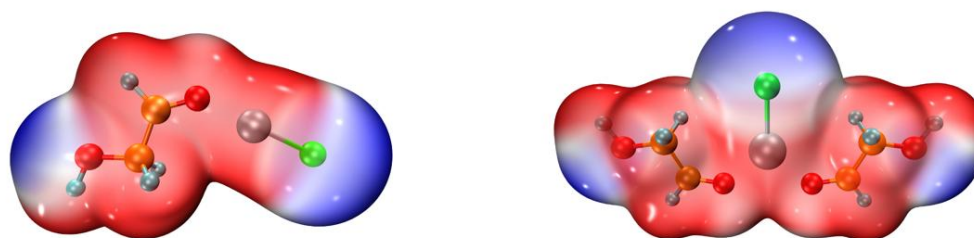
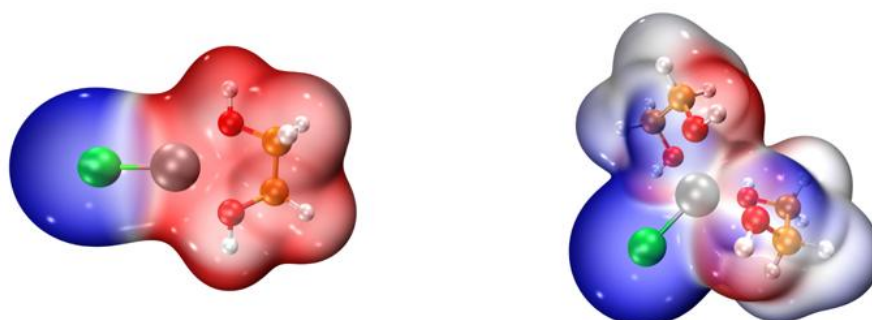


Figure S8. Second coordination mode:  $[ZnCl(EG)]^+$  and  $[ZnCl(EG)_2]^+$  cations using two -OH groups of EG to coordinate with  $Zn^{2+}$ .



	<b>Bonding Strength <math>\Delta E</math> (eV)</b>	<b>Gibbs Free Energy <math>\Delta G</math> (eV)</b>
<b>Zn-Cl with one EG</b>	<b>4.27838670</b>	<b>-2.532721246</b>
<b>Zn-Cl with two EG</b>	<b>1.99314142</b>	<b>-3.696304582</b>

Figure S9. Bond strength and Gibbs free energy of  $[\text{ZnCl}(\text{EG})]^+$  and  $[\text{ZnCl}(\text{EG})_2]^+$  cations using one  $-\text{OH}$  group of EG to coordinate with  $\text{Zn}^{2+}$ .



	<b>Bonding Strength <math>\Delta E</math> (eV)</b>	<b>Gibbs Free Energy <math>\Delta G</math> (eV)</b>
<b>Zn-Cl with one EG</b>	<b>3.91106716</b>	<b>-3.32953235</b>
<b>Zn-Cl with two EG</b>	<b>1.74114857</b>	<b>-4.44447687</b>

**Figure S10.** Bond strength and Gibbs free energy of  $[\text{ZnCl}(\text{EG})]^+$  and  $[\text{ZnCl}(\text{EG})_2]^+$  cations using two -OH groups of EG to coordinate with  $\text{Zn}^{2+}$ .

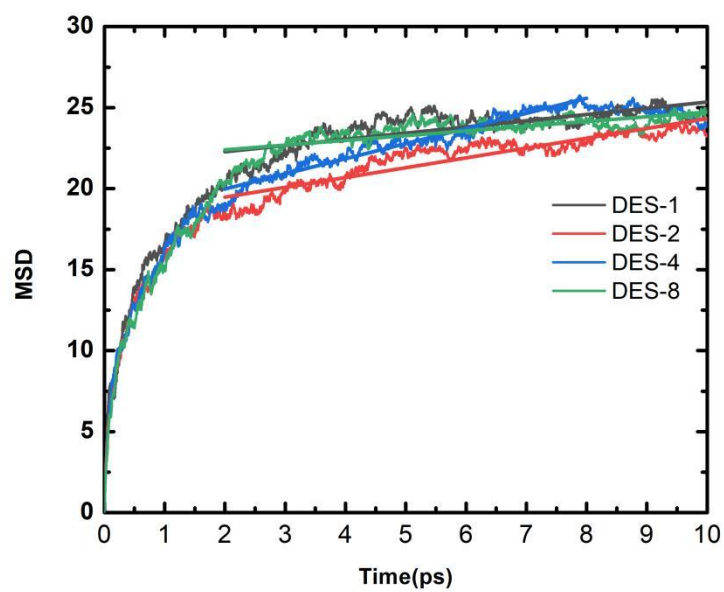


Figure S11. Mean squared displacement (MSD) of the  $\text{Zn}^{2+}$  in DES-1, DES-2, DES-4, and DES-8 electrolytes.

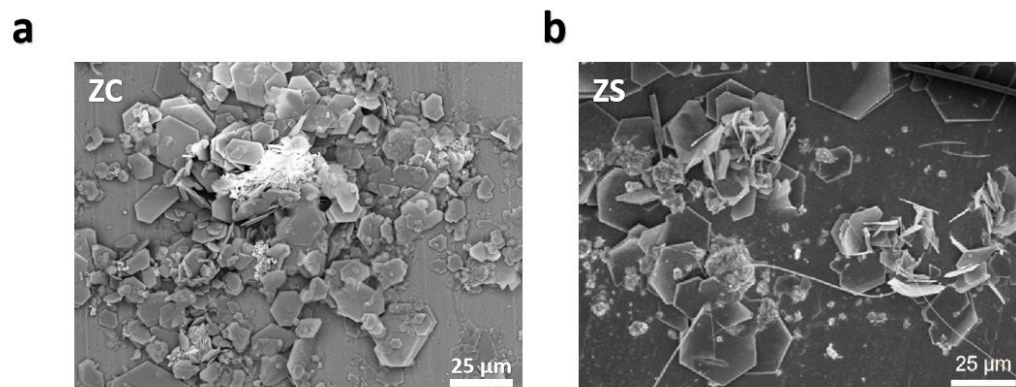


Figure S12. SEM images of Zn plated on Ti foil at  $1 \text{ mAh cm}^{-2}$  through the Ti||Zn cells with (a) ZC, and (b) ZS aqueous electrolytes.

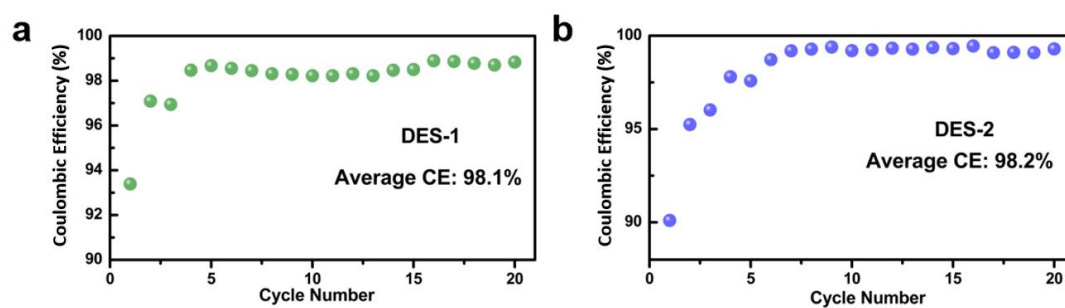


Figure S13. Zn plating/stripping Coulombic efficiency of the Ti||Zn cells using (a) DES-1 and (b) DES-2 electrolytes at a current density of  $1 \text{ mA cm}^{-2}$  and a capacity of  $1 \text{ mAh cm}^{-2}$ .

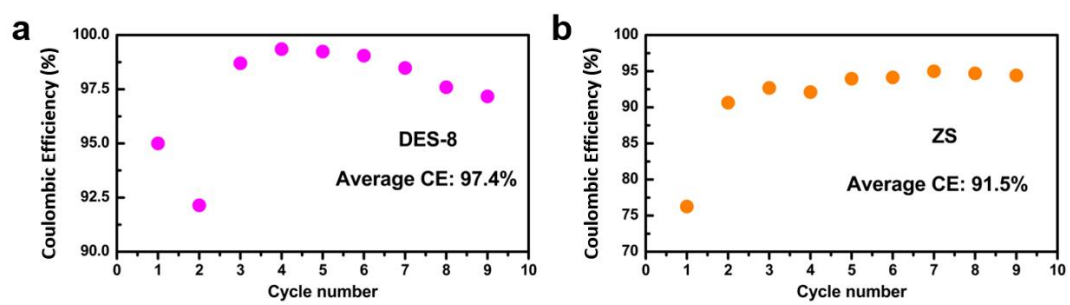


Figure S14. Zn plating/stripping Coulombic efficiency of the Ti||Zn cells with (a) DES-8 and (b) ZS electrolytes at a current density of  $1 \text{ mA cm}^{-2}$  and a capacity of  $1 \text{ mAh cm}^{-2}$ .

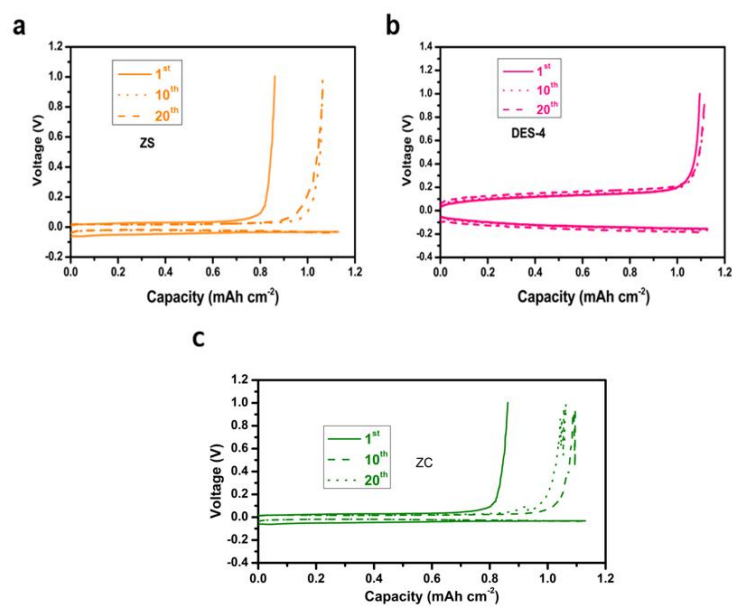


Figure S15. Voltage profiles of Ti||Zn cells with (a) ZS, (b) DES-4, and (c) ZC electrolytes at a current density of 1 mA cm<sup>-2</sup> and a capacity of 1 mA h cm<sup>-2</sup>.

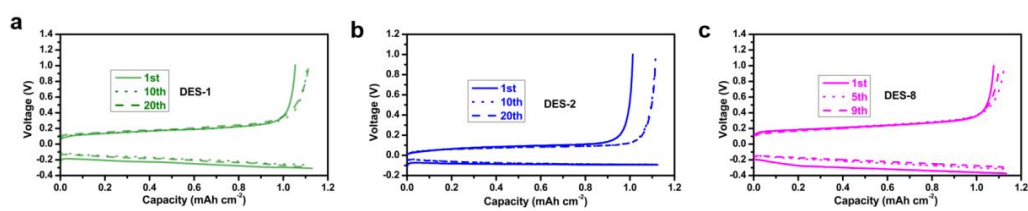
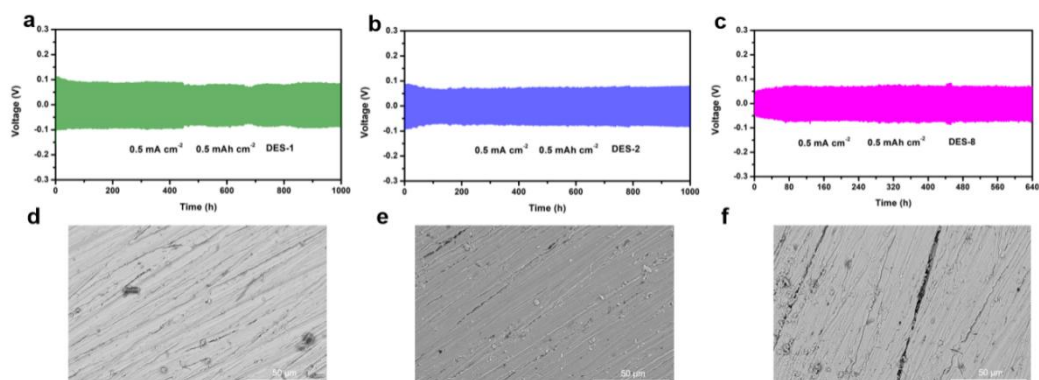


Figure S16. Voltage profiles of Ti||Zn cells with (a) DES-1, (b) DES-2, and (c) DES-8 electrolytes at a current density of 1 mA cm<sup>-2</sup> and a capacity of 1 mAh cm<sup>-2</sup>.



**Figure S17.** Galvanostatic Zn plating/stripping of Zn||Zn symmetrical cells with (a) DES-1, (b) DES-2, and (c) DES-8 electrolytes at a current density of  $0.5 \text{ mA cm}^{-2}$  and a capacity of  $0.5 \text{ mAh cm}^{-2}$ . SEM images of the Zn electrodes from Zn||Zn symmetrical cells with (d) DES-1, (e) DES-2, and (f) DES-8 electrolytes after 50 Zn plating/stripping cycles (current density:  $0.5 \text{ mA cm}^{-2}$ , capacity:  $0.5 \text{ mAh cm}^{-2}$ ).

The Zn||DES-1||Zn cell delivers a steady voltage hysteresis of  $\sim 100 \text{ mV}$  vs.  $\text{Zn/Zn}^{2+}$  over more than 1000 h, the Zn||DES-2||Zn cell delivers a steady voltage hysteresis of  $\sim 90 \text{ mV}$  vs.  $\text{Zn/Zn}^{2+}$  over more than 1000 h and the Zn||DES-8||Zn cell also delivers a steady voltage hysteresis of  $\sim 60 \text{ mV}$  vs.  $\text{Zn/Zn}^{2+}$  over more than 640 h.

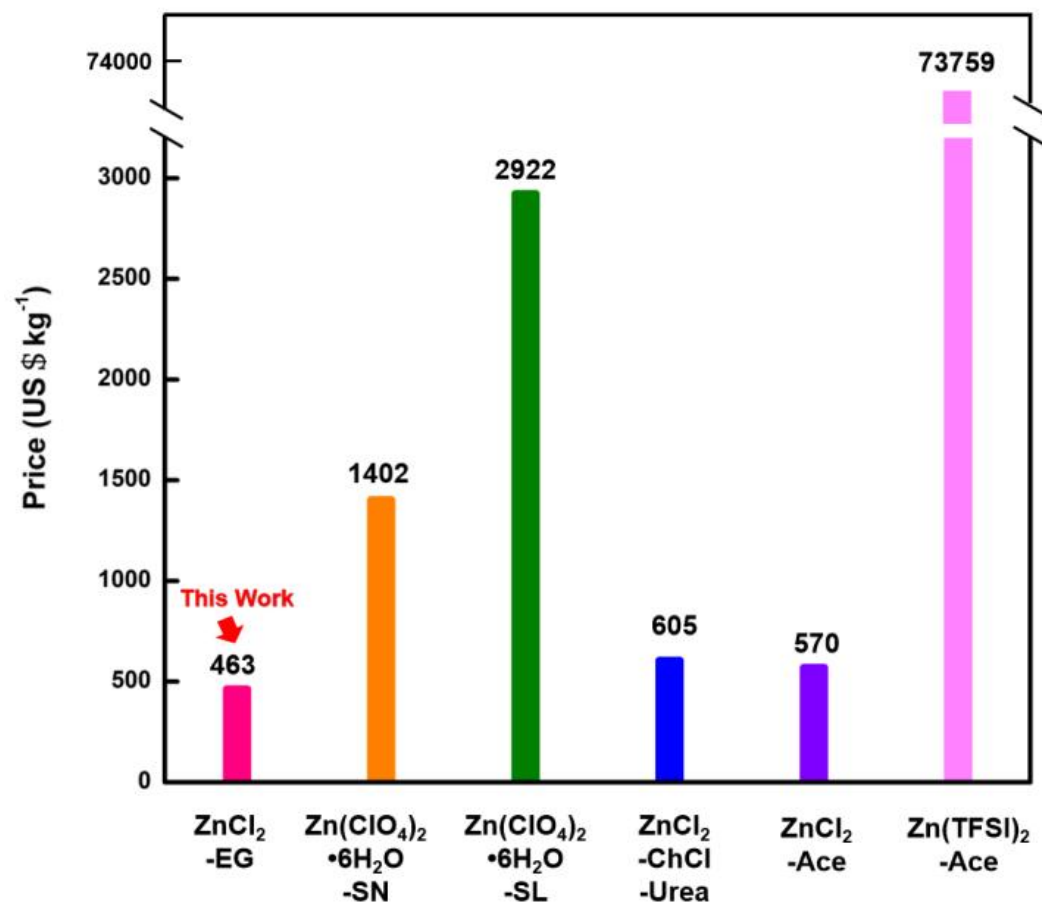


Figure S18. Price of various eutectic electrolytes for ZIBs.

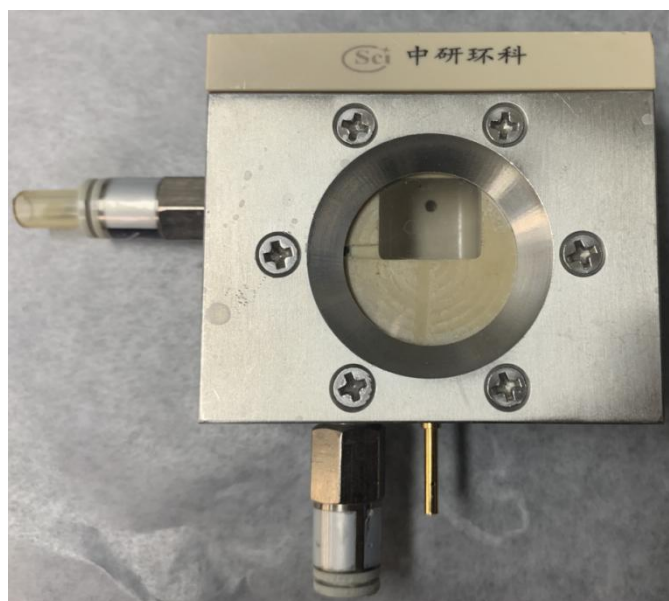
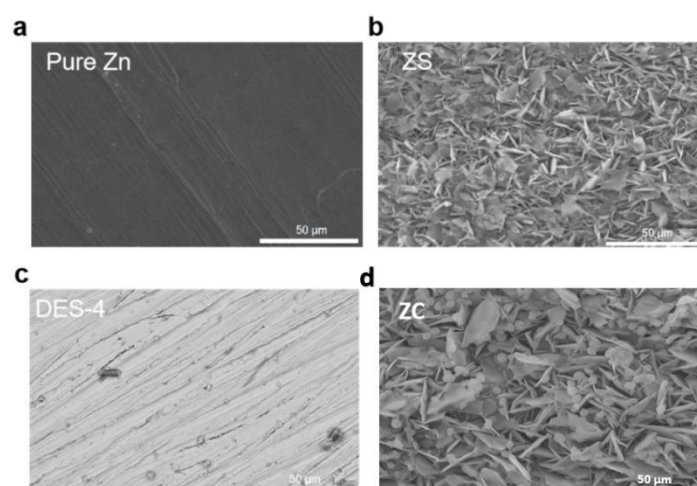
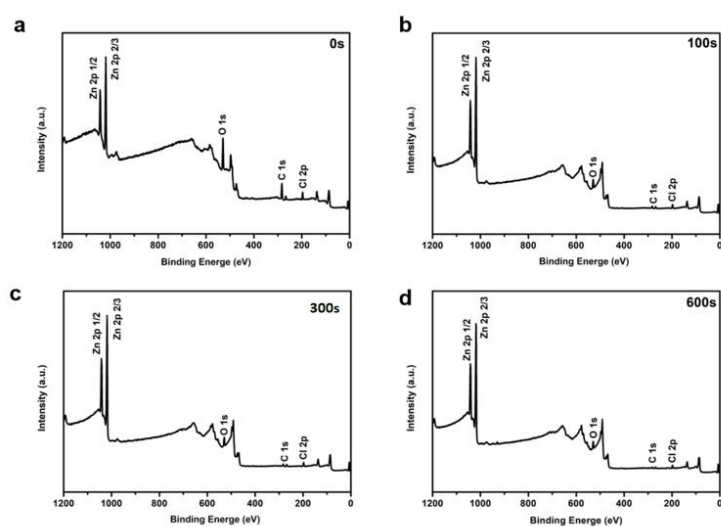


Figure S19. Optical cells for *in-situ* observation of the Zn plating process.



**Figure S20.** SEM images of (a) pure Zn and Zn anode after 50 cycles in (b) ZS, (c) DES-4, and (d) ZC electrolytes using Zn||Zn symmetrical cells at a current density  $0.5 \text{ mA cm}^{-2}$  and a capacity of  $0.5 \text{ mAh cm}^{-2}$ .



**Figure S21.** XPS survey spectra of the Zn anode after 50 cycles in Zn||Zn symmetrical cells with DES-4 electrolyte at a current density 0.5 mA cm<sup>-2</sup> and a capacity of 0.5 mAh cm<sup>-2</sup> after Ar<sup>+</sup> sputtering for (a) 0 s, (b) 100 s, (c) 300 s, and (d) 600 s.

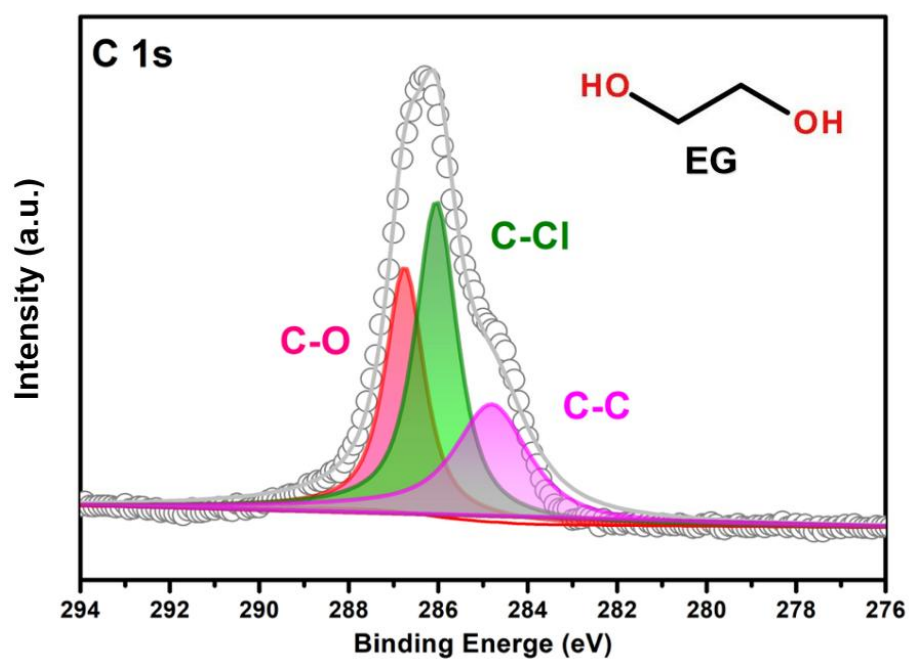
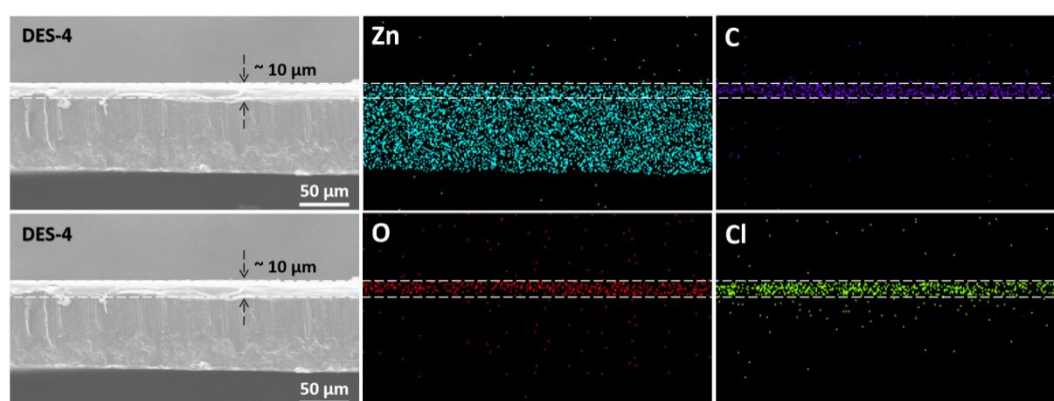
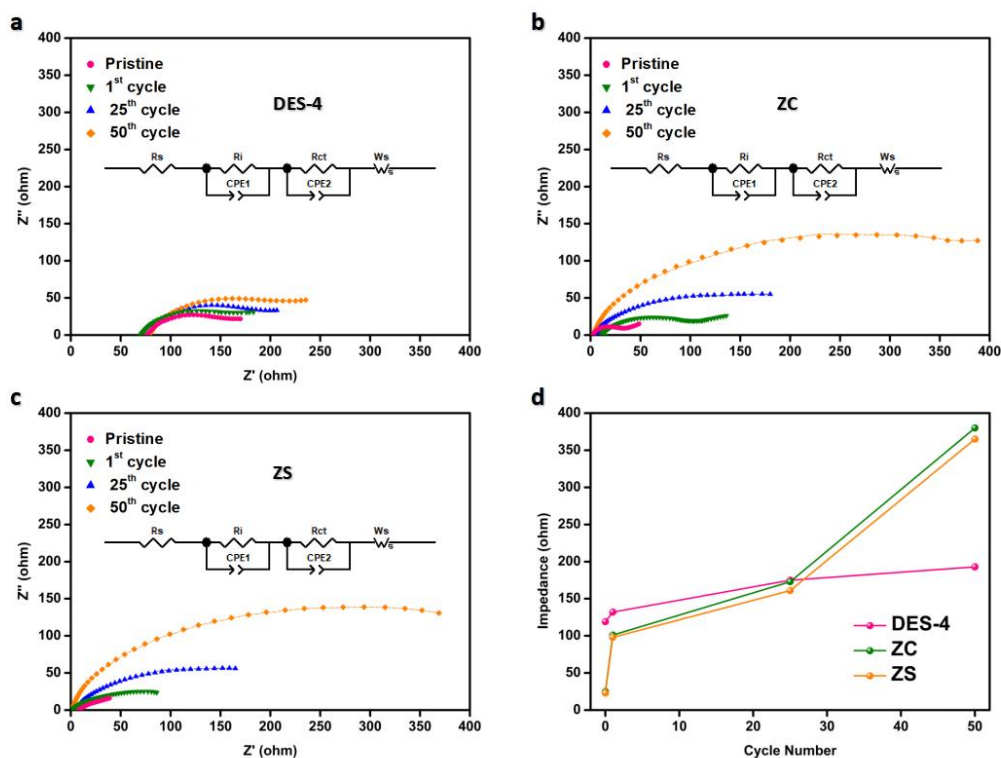


Figure S22. C 1s XPS spectrum of the surface of Zn anode cycled in DES-4 electrolyte at a current density  $0.5 \text{ mA cm}^{-2}$  and a capacity of  $0.5 \text{ mAh cm}^{-2}$  after 50 cycles.



**Figure S23.** Cross-sectional SEM images and EDS mappings of the Zn anode after 50 cycles in Zn||Zn symmetrical cells with DES-4 electrolyte at a current density  $0.5 \text{ mA cm}^{-2}$  and a capacity of  $0.5 \text{ mAh cm}^{-2}$ .



**Figure S24.** The Zn-electrolyte interface stability in different electrolytes. EIS data measured with Zn/Zn symmetric cells in (a) DES-4 and (b) ZC, and (c) ZS at different galvanostatic cycles at  $0.5 \text{ mA cm}^{-2}$ . Scatter plots and dashed lines denote experimental spectra and fitting curves of impedance, respectively. Insets in (a), (b), and (c) exhibit the equivalent circuit model of EIS.  $R_s$  stands for the electrolyte bulk resistance.  $R_i$  and  $CPE1$  are the interface resistance and its related double-layer capacitance, which correspond to the semicircle at high frequencies,  $R_{ct}$  and  $CPE2$  represent the charge transfer resistance and its related double-layer capacitance, which correspond to the semicircle at medium frequencies, and  $W_s$  represents the Warburg impedance related to the diffusion of Zn-ions, which is indicated at low frequencies.<sup>[9]</sup> (d) The evolution of the charge-transfer resistance in different electrolytes.

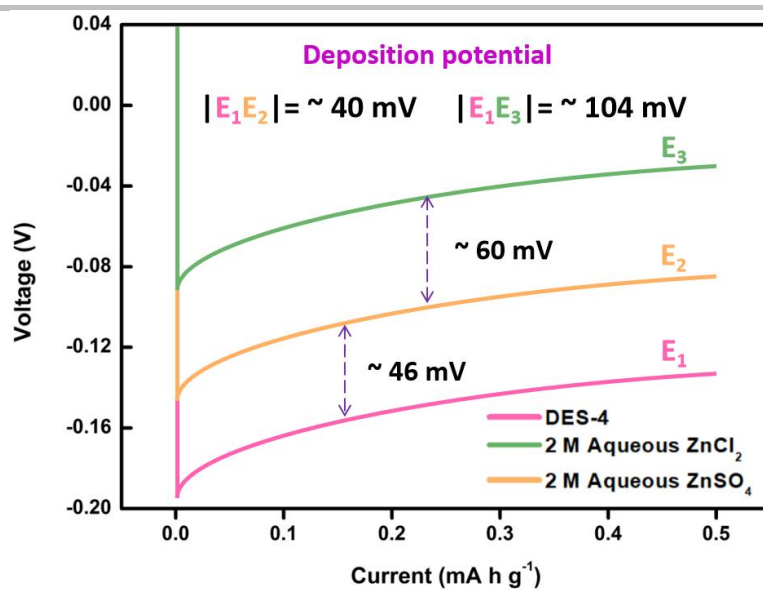
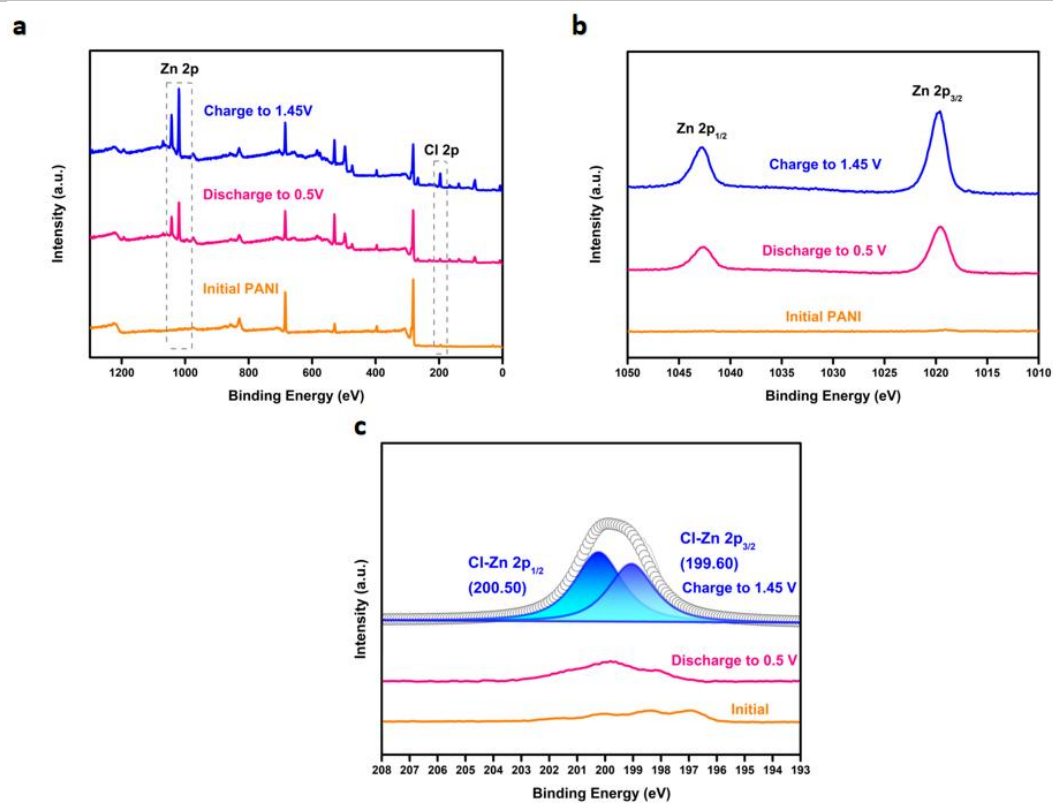


Figure S25. The potentials for Zn deposition on Ti substrate at  $0.5 \text{ mA cm}^{-2}$ .



**Figure S26.** (a) XPS survey spectra of PANI cathode at different states. (b) Zn 2p XPS spectra of PANI cathode at different states. (c) Cl 2p XPS spectra of PANI cathode at discharge and charge states.

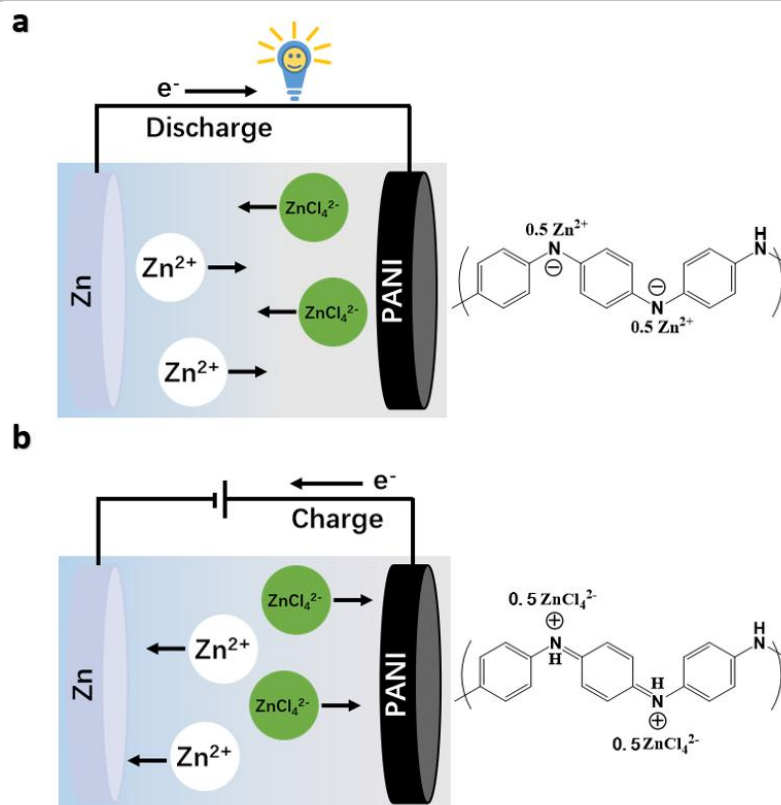


Figure S27. (a) Discharge and (b) charge mechanism of PANI||DES-4||Zn full cell.

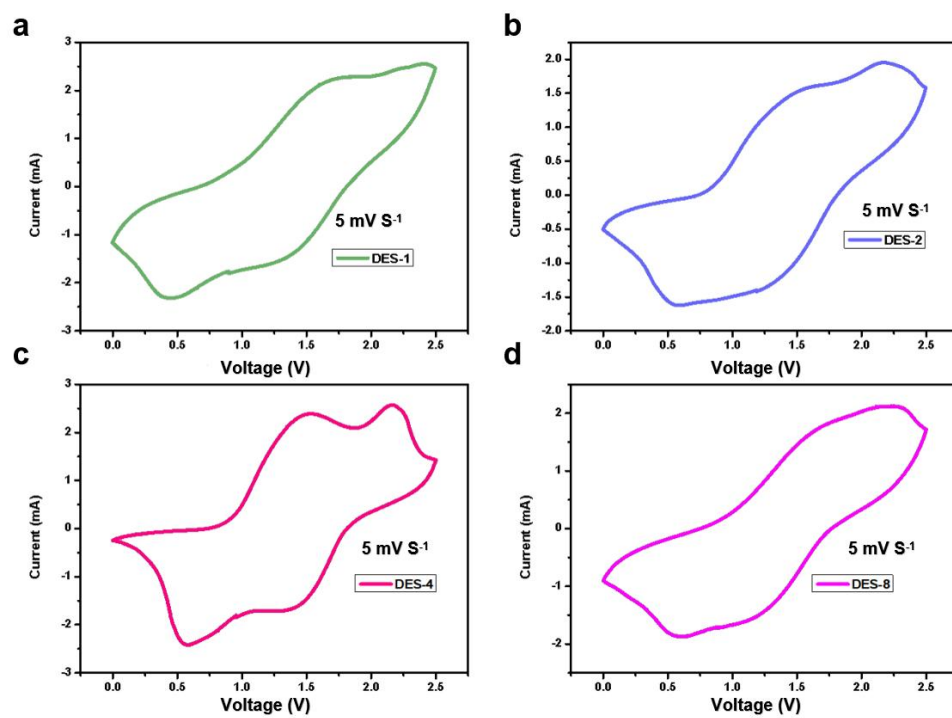
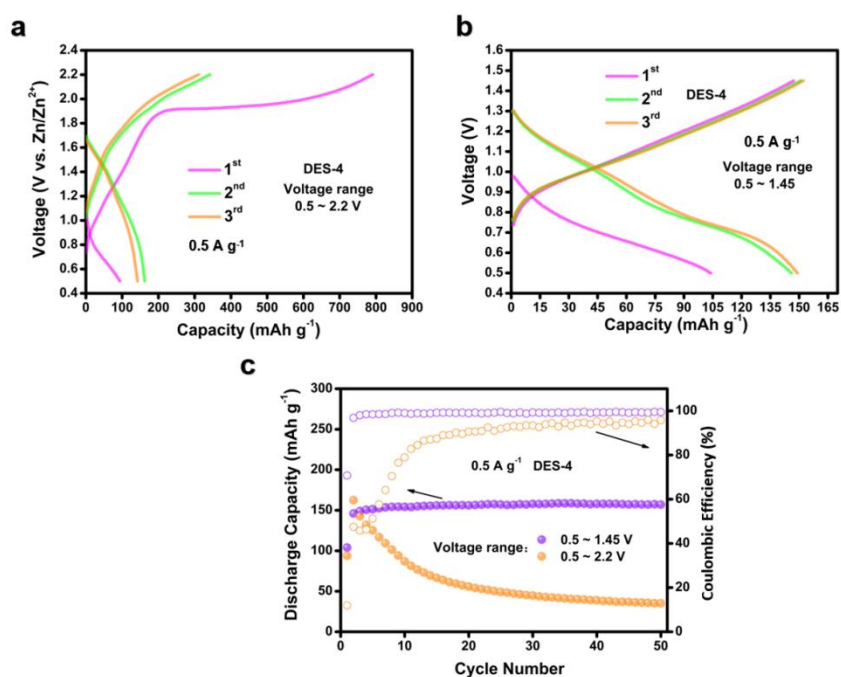


Figure S28. CV curves of the PANI||Zn cells with (a) DES-1, (b) DES-2, (c) DES-4, and (d) DES-8 electrolytes at a scan rate of 5 mV s<sup>-1</sup>.



**Figure S29.** Charge/discharge curves of the PANI||Zn coin cells with DES-4 electrolyte at 0.5 A g<sup>-1</sup> in the voltage window of (a) 0.5 – 1.45 V and (b) 0.5 – 2.2 V. (c) Cycling performances of the PANI||Zn coin cells with DES-4 electrolyte at 0.5 A g<sup>-1</sup>.

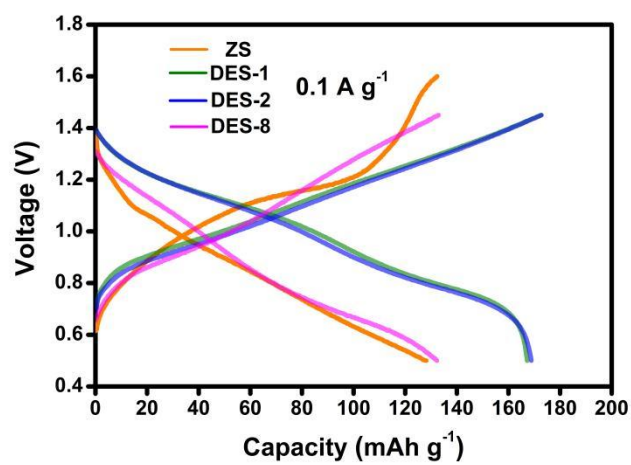
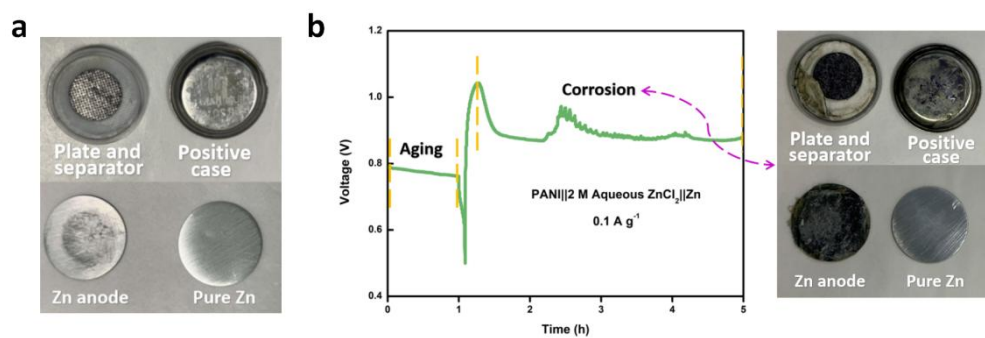


Figure S30. Charge/discharge curves of the PANI||Zn coin cells with different electrolytes at 0.1 A g<sup>-1</sup>. For DES electrolytes, the cells are cycled in the voltage range of 0.5 – 1.45 V, for aqueous ZS electrolyte, the cell is cycled in the voltage range of 0.5 – 1.6 V.



**Figure S31.** (a) Photo of the disassembled PANI||DES-4||Zn coin cell after 50 cycles (no corrosion). (b) Work curves of PANI||Zn coin cells with ZC at 0.1 A g<sup>-1</sup> in the voltage range of 0.5 – 1.45 V showing the corrosion situation.

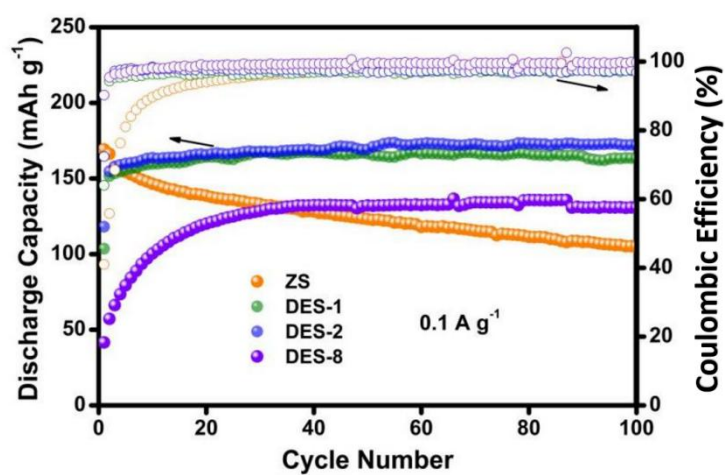


Figure S32. Cycling performances of the PANI||Zn coin cells with DES-1, DES-2, DES-8, and ZS electrolytes at 0.1 A g<sup>-1</sup>.

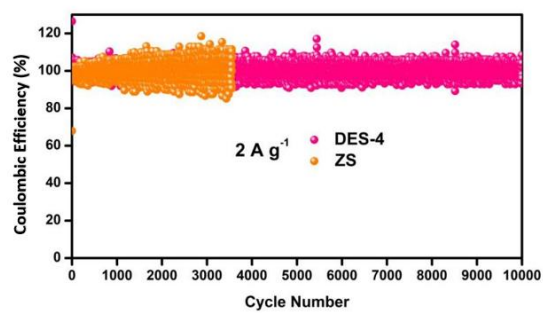


Figure S33. Coulombic efficiency of PANI||Zn cells with ZS and DES-4 electrolytes at  $2 \text{ A g}^{-1}$ .

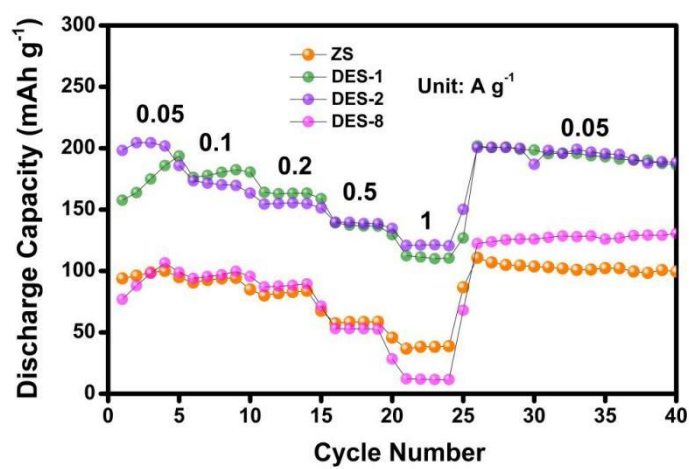


Figure S34. Rate performances of the PANI||Zn coin cells with different electrolytes.

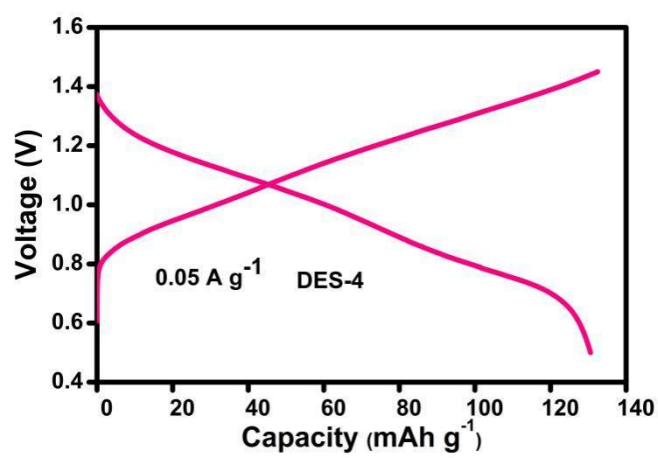


Figure S35. Charge/discharge curves at 0.05 A g<sup>-1</sup>.

Table S1 Comparison of various eutectic electrolytes for ZIBs.

Eutectic electrolyte	ESW	Ionic conductivity (mS cm <sup>-1</sup> )	Cycle stability in Zn//Zn symmetry (0.5 mA cm <sup>-2</sup> , 0.5 mAh cm <sup>-2</sup> )	Electrochemical performance of full ZIBs	SEI formation	Refs.
ZnCl <sub>2</sub> /EG	2.15 V vs. SCE	1.15	3200 h	PANI//Zn cell capacity retention of 78 % after 10,000 cycles at 2 A g <sup>-1</sup>	Cl-rich	This Work
ZnCl <sub>2</sub> /ChCl/Urea	1.4 V vs. Ag/AgCl	0.5	300 h	δ-MnO <sub>2</sub> //Zn cell capacity retention of 60 % after 150 cycles at 0.1 A g <sup>-1</sup>	/	10
Zn(TFSD) <sub>2</sub> /Ace	2.4 V vs. Zn/Zn <sup>2+</sup>	0.31	2000 h	V <sub>2</sub> O <sub>5</sub> //Zn cell capacity retention of 92.8 % after 800 cycles at 1 A g <sup>-1</sup>	F-rich	9
Zn(ClO <sub>4</sub> ) <sub>2</sub> /6H <sub>2</sub> O/SN	2.55 V vs. Zn/Zn <sup>2+</sup>	5.52	800 h 0.05 mA cm <sup>-2</sup> , 0.5 mAh cm <sup>-2</sup>	PDB//Zn cell capacity retention of 85.4 % after 3,500 cycles at 0.3 C	/	11
Zn(ClO <sub>4</sub> ) <sub>2</sub> /6H <sub>2</sub> O/SL	2.53 V vs. Zn/Zn <sup>2+</sup>	2	800 h	PANI//Zn cell capacity retention of 78 % after 2,500 cycles at 3 A g <sup>-1</sup>	/	12

## References

- [1] E. L. Smith, A. P. Abbott, K. S. Ryder, *Chem. Rev.* **2014**, *114*, 11060-11082.
- [2] L. Zhang, C. Zhang, Y. Ding, K. Ramirez-Meyers, G. Yu, *Joule* **2017**, *1*, 623-633.
- [3] C. Zhang, L. Zhang, G. Yu, *Acc. Chem. Res.* **2020**, *53*, 1648-1659.
- [4] D. V. Wagle, H. Zhao, G. A. Baker, *Acc. Chem. Res.* **2014**, *47*, 2299-2308.
- [5] A. P. Abbott, J. C. Barron, K. S. Ryder, D. Wilson, *Chem. Eur. J.* **2007**, *13*, 6495-6501.
- [6] F. Wan, L. Zhang, X. Wang, S. Bi, Z. Niu, J. Chen, *Adv. Funct. Mater.* **2018**, *28*, 1804975.
- [7] Q. Zhang, Y. Ma, Y. Lu, L. Li, F. Wan, K. Zhang, J. Chen, *Nat. Commun.* **2020**, *11*, 4463.
- [8] J. Cui, Z. Guo, J. Yi, X. Liu, K. Wu, P. Liang, Q. Li, Y. Liu, Y. Wang, Y. Xia, J. Zhang, *ChemSusChem* **2020**, *13*, 2160-2185.
- [9] H. Qiu, X. Du, J. Zhao, Y. Wang, J. Ju, Z. Chen, Z. Hu, D. Yan, X. Zhou, G. Cui, *Nat. Commun.* **2019**, *10*, 5374.
- [10] Kao-ian, W.; Pornprasertsuk, R.; Thamyongkit, P.; Maiyalagan, T.; Kheawhom, S. *J. Electrochem. Soc.* **2019**, *166*, A1063-A1069.
- [11] W. Yang, X. Du, J. Zhao, Z. Chen, J. Li, J. Xie, Y. Zhang, Z. Cui, Q. Kong, Z. Zhao, C. Wang, Q. Zhang, G. Cui, *Joule* **2020**, *4*, 1557-1574.
- [12] X. Lin, G. Zhou, M. J. Robson, J. Yu, S. C. T. Kwok, F. Ciucci, *Adv. Funct. Mater.* **2022**, *32*, 2109322.

## Author Contributions

L.M. and L.Z. supervised the project. L.G. designed and synthesized the eutectic electrolyte and performed most of the experiments. L.G., J.M. and P.X. performed NMR, FT-IR and Raman tests. L.G., Z.X. and K.H. performed the XPS and SEM measurements. L.G., C.H., P.X. and L.Z. conducted and discussed the theoretical calculations. L.G. wrote the initial draft of the manuscript. All authors discussed the results and edited the manuscript.